CHAPTER 4

CHAPTER 4

ASSESSMENT OF BIOMASS GASIFIER OPERATING PERFORMANCE

Evaluation of performance of gasifier utilizing a variety of biomass feedstock is essential in planning of a biomass gasification based electricity generation system for a region. Performance evaluation is based on the estimation of output gas composition and calorific value of the output gas. The reactor design and operating parameters influence the gasifier performance. Mathematical modeling serves as an important route to study the gasifier behaviour in order to optimize its design and operation in comparison to physical experimentation which is both time consuming and uneconomical. For example, commissioning a gasifier at a given location requires performance evaluation based on the different feedstock available in the region. Experimentation utilizing the array of biomass puts time constraints on the planning process along with increased financial involvement. On the other hand, if we have a mathematical model of the system then we can easily find out how the system will perform in accordance with the characteristics of the available feedstock. Mathematical models give a realistic representation of the chemical and physical phenomena occurring inside the gasifier. Equilibrium modeling, kinetic modeling, computational fluid dynamic (CFD) modeling and artificial neural network (ANN) modeling are the some of the techniques used in biomass gasification study. ANN and Kinetic modeling has been considered for the present study. Choice of the techniques has been discussed in Chapter 2. The following sections discusses the development of ANN and Kinetic models of fixed bed downdraft gasifiers.

4.1 Development of ANN models of biomass gasification (This Section is adapted from Author's own publication [1])

In the present study an attempt has been made to develop a multi-layer perceptron (MLP) based ANN model of the biomass gasification process in a fixed bed downdraft gasifier. The objective of the study is to develop ANN model and utilize it in predicting the product gas composition in terms of percentage composition of the product gas species for variations in the operating parameters. Further, it is attempted to determine the relative influence of some specific operating parameters on output gas.

4.1.1 Topology of the ANNs

An ANN based model for fixed bed downdraft type of gasifiers is developed to study gasification behaviour in terms of product gas composition. An ANN is an architecture consisting of a large number of neurons organized in different layers and the neurons of one layer are connected to those of another layer by means of weights and it can be trained to perform a particular task by making proper adjustment of its connecting weights, bias and architecture [2]. In this study, ANN models were developed in the MATLAB environment using the Neural Network Toolbox (nntool). Fig. 4.1 represents the architecture of the ANN models developed for each output (CH_4, CO, CO_2 and H_2). Each ANN has one input layer with six variables *viz.* C (wt% dry basis), H (wt% dry basis), O (wt% dry basis), ash (wt% dry basis), MC (%), and reduction zone temperature, T_R (°C) with one hidden layer and one output.

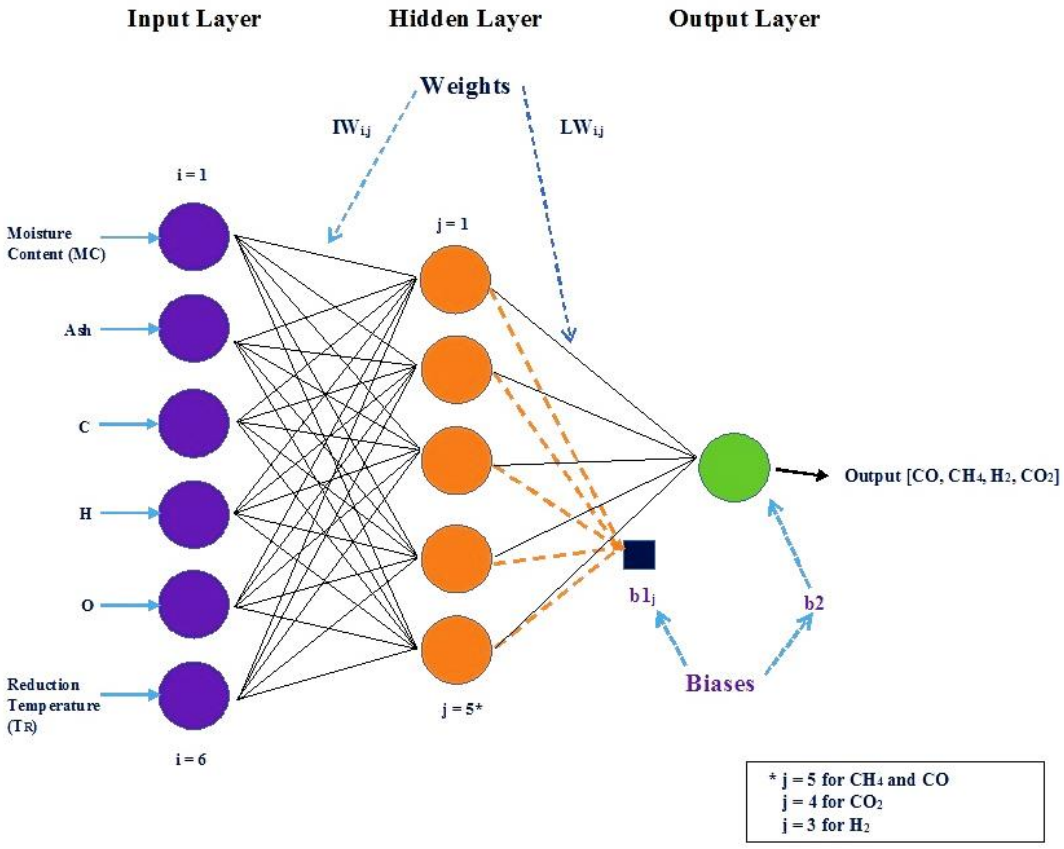

Fig. 4.1 ANN architecture to predict the gas components for fixed bed downdraft gasifiers

In the models, the activation function used in the hidden layers was a hyperbolic tangent sigmoid function (TANSIG). This transfer function results in an output that

lies in the range of (-1.0 to 1.0) and generally used for back propagation networks. The input-output relationship for this transfer function is given by Eq. 4.1.

$$U_k = \frac{e^{a(V_k)} - e^{-a(V_k)}}{e^{a(V_k)} + e^{-a(V_k)}} \quad \text{---- 4.1}$$

where, V_k and U_k are the input and output of the k^{th} neuron and 'a' represents the coefficient of transfer function. Plot of the hyperbolic tangent sigmoid function is shown in Fig. 4.2.

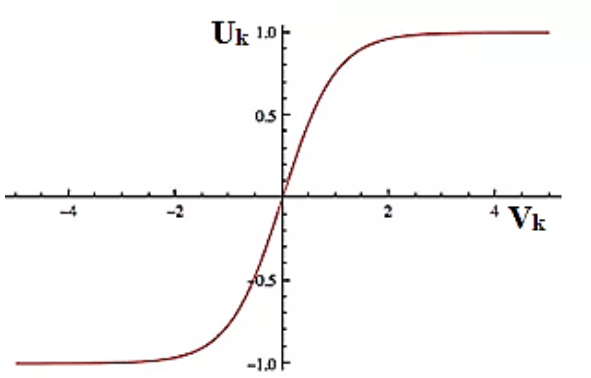

Fig. 4.2 Tan-sigmoid transfer function

The linear transfer function (PURELIN) was used in the output layer. The output of this transfer function is made equal to its input and it lies in the range of (-1.0 to 1.0). The input-output relationship of this transfer function is expressed by Eq. 4.2. Plot of the linear transfer function is shown in Fig. 4.3.

$$U_k = V_k \quad \text{---- 4.2}$$

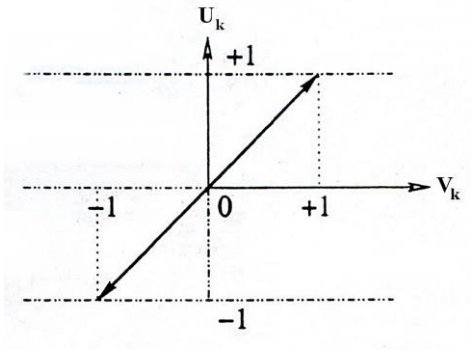

Fig. 4.3 Linear transfer function

In order to find out the most appropriate or best solution, a large number of different ANN models were developed with different number of hidden layers and different number of neurons for each hidden layer. The optimum solution was selected by

minimizing the Mean Square Error (MSE). The best results were considered as one hidden layer with five neurons in the case of CH_4 and CO, one hidden layer with four neurons in the case of CO_2 and one hidden layer with three neurons in the case of H_2.

4.1.2 Data selection for the model

An extensive literature review was conducted to obtain experimental data for biomass gasification under atmospheric pressure in downdraft fixed bed gasifiers. In order to maintain homogeneity in the different input variables considered for the development of the ANN based model, only experimental data pertaining to woody biomass and pellet gasification were considered. As results from large scale gasifiers (>100 kW) cannot be compared with results from small scale gasifiers, experimental data from small scale gasifiers only were incorporated in the development of the model. Table 4.1 lists out the experimental works utilised in development of the model.

Table 4.1 Experimental data used in formulation of the ANN models

Sl. No.	Author(s)	Feedstock Used	Number of data sets used
1	Antonopoulos et al. [3]	Olive wood, miscanthus and cardoon	4
2	Dogru [4]	Hazelnut shells	3
3	Erlich and Fransson [5]	Empty fruit brunch, Bagasse, Wood	5
4	Gai and Dong [6]	Corn straw pelletes	5
5	Janajreh and Al Shrah [7]	Wood chips	3
6	Jaojaruek et al. [8]	Eucalyptus wood	3
7	Jordan and Akay [9]	Fuel Cane Bagasse Pellet	3
8	Kallis et al. [10]	Miscanthus and bioethanol waste pellets	3
9	Lapuerta et al.[11]	Wood Chips	3
10	Lv et al. [12]	Pine wood blocks	3
11	Melgar et al. [13]	Rubber Wood	5
12	Sharma [14,15]	Kiker wood, Douglas Fir Bark	3
13	Sheth and Babu [16]	Sesame or rose wood	3
14	Tinaut et al. [17]	Pine Bark	3
15	Van de steene et al. [18]	Wood chips	5
16	Varunkumar et al. [19]	Wood	3
17	Warnecke [20]	Hazelnut shells	3
18	Wei et al. [21]	Hardwood chips blended with crude glycerol	3

The data set for the downdraft fixed bed gasifiers contain data from 63 different experimental runs [3-21] for various feedstock. Feedstock characteristics *viz.* moisture (MC), ash, C, H and O content along with reduction temperature (T_R) were

considered to be the input variables in the formulation of the ANN models. Fixed carbon (FC) and volatile matter (VM) as stated by Brown et al. [22] based on the previous works of van Krevelen [23] and Jenkins et al. [24] are considered as dependent variables because the FC ratio is proportional to both the H/C and O/C ratios. Thus, FC and VM were excluded from the input variables. Nitrogen and sulphur content were also not considered as they are assumed to have little influence in the production of gas species *viz.* CO, CO_2, H_2 and CH_4. Table 2 lists the characteristics of the input and output variables obtained from the experimental data published in standard literature.

Table 4.2 Characteristics of input and output variables in the ANN models

Input Variables to the ANN's	**Range**
C (wt% dry basis)	43.83 - 53.4
H (wt% dry basis)	5.42 - 7.18
O (wt% dry basis)	37.24 - 45.83
Ash (wt% dry basis)	4.25 - 9.48
Moisture Content (%)	4.20 - 14.70
Reduction Temperature (°C)	600 - 1206
Output Variables for the ANN's	
CO content (%)	10.83 - 24.00
CH_4 content (%)	2.00 - 6.91
H_2 content (%)	9.30 - 19.00
CO_2 content (%)	10.02 - 23.93

4.1.3 Training, validation and prediction ability of the models

In order to check the robustness, validation and prediction ability of the models, the database was divided into two parts as training (70%) and validation-testing (30%) sub-sets. The training function used in the models were based on the TRAINLM function which updates the weight and bias values according to Levenberg-Marquardt optimization. This function is often the fastest backpropagation algorithm. Also, the Gradient descent with momentum weight and bias learning function (LEARNGDM) was used to minimise the errors. This function calculates the weight change for a given neuron from the neuron's input and error, the weight (or bias), learning rate, and momentum constant, according to gradient descent with momentum backpropagation. Training and validation-test subsets were randomly selected from the available database. Details of the ANN models are summarised in Table 4.3.

Table 4.3 Details of ANN models

Sl. No.	Particulars	Specifications
1	Network type	Feed Forward Backpropagation
2	Training function or Training algorithm	Levenberg-Marquardt backpropagation (TRAINLM)
3	Adaption learning function	Gradient Descent with Momentum Weight and Bias (LEARNGDM)
4	Performance function	Mean Square Error (MSE)
5	Transfer function	Hyperbolic Tangent Sigmoid (TRANSIG)
6	Data division	Random (Dividerand)
7	Number of input layer unit	6
8	Number of output layer unit	1
9	Number of hidden layer	1
10	Number of hidden layer neuron	5 each for CH_4 and CO, 4 for CO_2 & 3 for H_2
11	Number of epoch (Learning cycle)	1000 iterations

The prediction ability of the ANNs were statistically appraised by root mean square error (RMSE) and absolute fraction of variance (R^2) which were calculated with the experimental values and networks predictions using equations 4.3 and 4.4, respectively.

$$RMSE = \left(\left(\frac{1}{p}\right)\sum_j |T_j - O_j|^2\right)^{\frac{1}{2}} \quad \text{---- 4.3}$$

$$R^2 = 1 - \left(\frac{\sum_j (T_j - O_j)^2}{\sum_j (O_j)^2}\right) \quad \text{---- 4.4}$$

where, p is the number of samples, T_j is the target (actual) value and O_j is the output (predicted) value.

4.1.4 Relative influence of input variables on model outputs

It is desirable to have an understanding of the influence of different input variables on the outputs of the model. Such knowledge would help in specifying optimum values of input variables for optimizing the performance of the gasifier. Influence of the input variables on the outputs was evaluated with the help of Garson equation which is based on neural net weight matrix [2]. Garson [2] proposed an equation that is based on the partitioning of connection weights. In the equation the numerator

describes the sums of absolute products of weights for each input and the denominator represents the sum of all weights feeding into hidden unit, taking the absolute values. The Garson equation, adapted to the present ANN topology is given in equation 4.5.

$$I_i = \frac{\sum_{j=1}^{j=n}\left(\left(\frac{|IW_{j,i}|}{\sum_{i=1}^{i=6}|IW_{j,i}|}\right).|LW_{j,i}|\right)}{\sum_{i=1}^{i=6}\left\{\sum_{j=1}^{j=n}\left(\left(\frac{|IW_{j,i}|}{\sum_{i=1}^{i=6}|IW_{j,i}|}\right).|LW_{j,i}|\right)\right\}} \quad \text{---- 4.5}$$

where, i is the input variables, j is the hidden layer neurons, I_i is the relative influence of the ith input variable on the output variable, $IW_{j,i}$ is the weight to jth neuron of hidden layer from ith input variable, $LW_{j,i}$ is the weight to output layer from jth neuron of hidden layer and n is the number of neurons (5 for CH_4 and CO, 4 for CO_2 and 3 for H_2). After computing the relative influence of the input variables on the output of each of the models, the input variables were ranked in descending order of magnitude. A comparative study of the variable ranking was then carried out.

4.1.5 Model output

Four neural networks with eight inputs, ten neurons in the hidden layer and one output each, were found to be efficient in predicting producer gas composition. The parameters ($IW_{j,i}$, $LW_{1,j}$, b_{1j}, b_2) of the best fit for each of the four ANN developed are shown in Appendix-I.

The simulated and experimental values of each output CO, CO_2, H_2 and CH_4 were compared satisfactorily through a linear regression model as shown in Fig. 4.4. It can be observed that R^2 values are higher than 0.99 in the cases of CH_4 and CO models and higher than 0.98 in the case of CO_2 and H_2 model. Further, the RMSE was found to be 0.0688 in the case of CO whereas it was 0.0523, 0.0915 and 0.0873 in the case of CH_4, H_2 and CO_2 respectively. After computing the limits for the statistical test of intercept and slope [25], the ANNs passed the test with 99.2% of confidence level. This test guarantees that whole ANN model, containing four ANNs, has a satisfactory level of confidence. Similar results were also reported by Puig-Arnavat et al. [26] for ANN models of fluidised bed gasifiers.

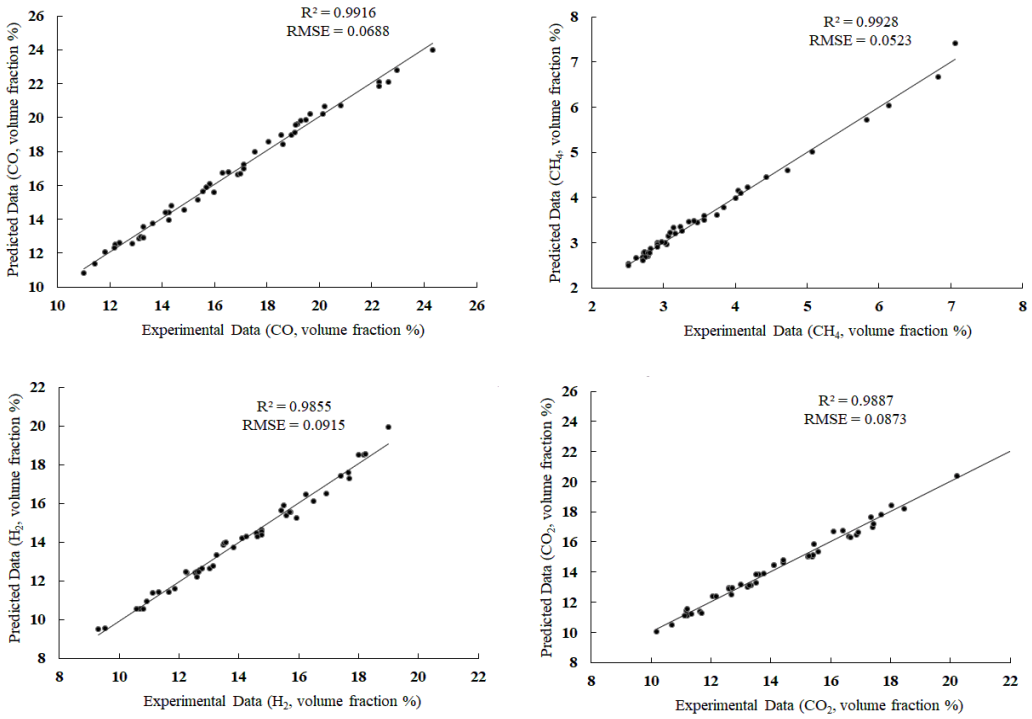

Fig. 4.4 Comparison between experimental and predicted data by the ANN models

The developed models were also compared with experimental results [27] outside the data set. The experimental results however had input values within the range of the input variables used in the development of the models. A comparative plot of the predicted and experimental result in shown in Fig. 4.5. Model results show good conformity with the experimental results with an average relative error of 2.65%.

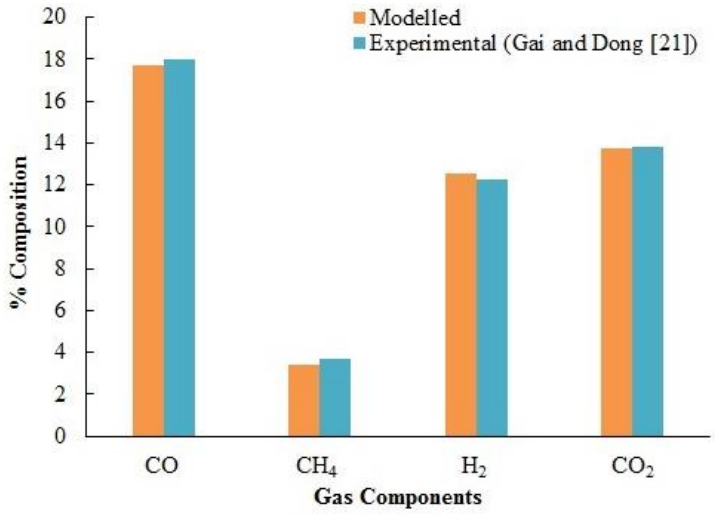

Fig. 4.5 Comparison between modelled data and experimental data.

The influence of the variables on the output prediction was calculated using the Garson's equation. Fig. 4.6 depicts the influence of input variables on each of the

output for the developed ANNs. Table 4.4 summarises the ranking of the variables in output prediction of the developed ANNs.

Table 4.4 Ranking of variables in output prediction for the ANN models

Rank	CO prediction	CH_4 prediction	H_2 prediction	CO_2 prediction
1	T_R	Ash	T_R	C
2	H	T_R	O	T_R
3	C	C	H	MC
4	Ash	H	MC	H
5	O	MC	C	Ash
6	MC	O	Ash	O

Percentage of influence of biomass composition (C, H and O) on end gas composition varies with the type of product gas. Further, T_R was the most important variable in CO and H_2 prediction while it was the second most important variable in CH_4 and CO_2 prediction.

Reduction zone temperature was found to be the most influential variable in conformation to the fact that increase in temperature leads to a noticeable increase in gas yield [28]. However, reactor temperature is significantly affected by MC of biomass due to heat required for evaporation of moisture [29]. MC was found to have a comparatively similar influence (9.24-11.09%) in the case of CO, CH_4 and H_2 while it had a relatively higher influence (17.08%) in the case of CO_2. H content was found to be the 2nd most influential variable in case of CO while it ranked 3rd in the case of H_2 and 4th in the case of CH_4 and CO_2 prediction. Ash content and C content were the most influential variable in the case of CH_4 and CO_2 prediction respectively. Ash content, however, showed relatively lower influence in the case of CO, H_2 and CO_2 where it ranked 4th, 6th and 5th respectively. Although higher ash content can lead to serious agglomeration, fouling, and corrosion in gasifiers, it is capable of influencing the gasification process as is evident from the results. However, the exact influencing phenomenon of ash on the gasification process may be a subject of further research. It may, however, be commented that each of the variables have a strong influence on the outputs with variations in the range of 8% to 31%.

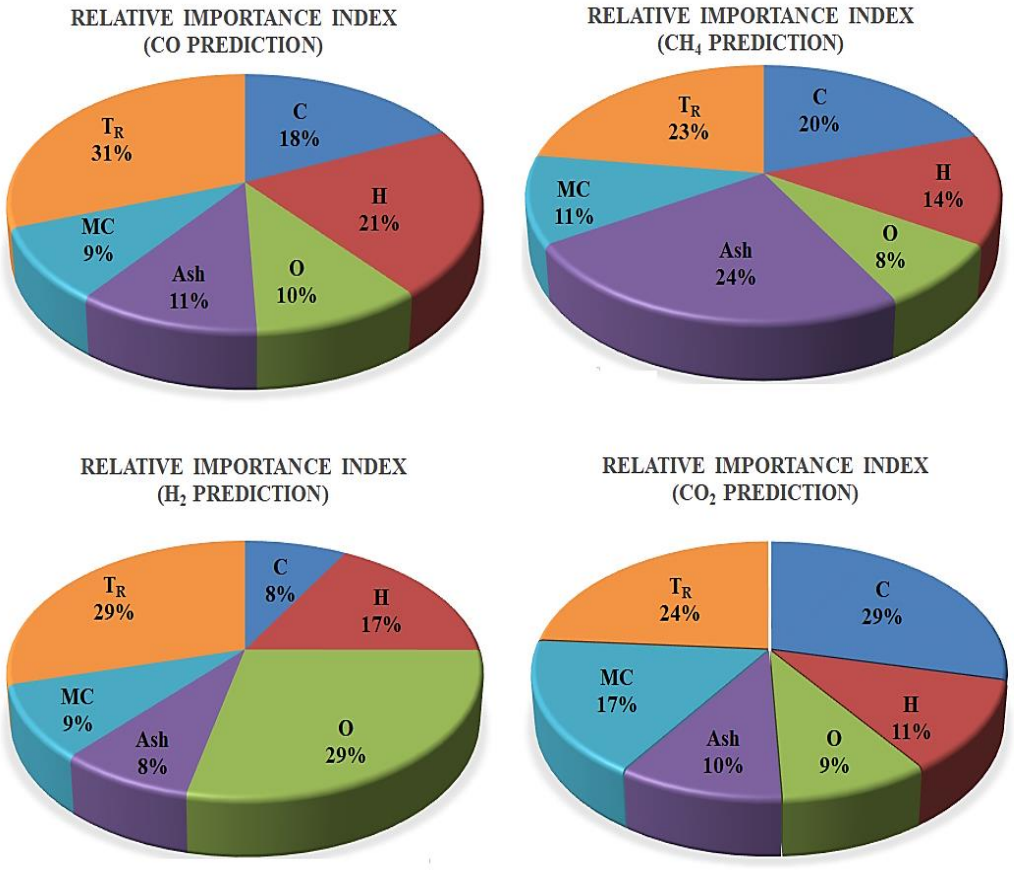

Fig. 4.6 Influence (relative %) of input variables on the different outputs of the ANN models.

The results show how the percentage composition of the major four gas species in producer gas can be successfully predicted by applying a neural network with one hidden neurons in the hidden layer and using backpropagation algorithm. The models are applicable for a wide variety of feedstock. However, expansion of the database with data from experimental runs for other varieties of feedstock becomes desirable to further increase the applicability of the models. The results also depict the relative importance of different operating parameters on the composition of the product gas species. The models are expected to have practical application in screening potential feedstock for biomass energy extension programmes based on gasification technology. However, in order to supplement the planning of a biomass gasification based electricity generation for a region, information of gasifier performance using more varieties of feedstock may be required. Keeping this in view, a kinetic model was also developed. The development of the model is discussed in the following section.

4.2 Development of Kinetic model of biomass gasification

In the gasification process, as the temperature increases, there is progressive domination of the thermal decomposition of biomass feedstock yielding char and volatiles. When these combustible products come in contact with oxygen in the air they get ignited. This provides the exothermic reactions to enhance further pyrolysis and the pyrolysis products are thermally cracked into lower molecular weight components [30]. In the present analysis, pyrolysis and oxidation of pyrolysis products in restricted air supply are described in a separate region denoted the pyro-oxidation zone. As the volatiles start depleting, the oxidation process start receding and the flames die down. This leads to char reduction with glowing surface [30]. The char reduction reactions are described separately in the char reduction zone. Thus, the model is developed in two stages. The first stage deals with the pyro-oxidation zone and the second stage with the char-reduction zone.

4.2.1 Initial conditions

The reduction zone model requires the concentration of gas species as an input parameter. This is obtained by describing the drying, pyrolysis and oxidation process simultaneously in pyro-oxidation zone. Char is assumed as pure carbon as the hydrogen and oxygen content decreases sharply with increase in temperature [31]. The pyro-oxidation process can be represented by a single reaction using Eq. 4.6.

$$C_6H_{HB}O_{OB} + \dot{w}H_2O + \dot{y}O_2 + 3.76\dot{y}N_2 = \dot{n}_{CO}CO + \dot{n}_{CO_2}CO_2 + \dot{n}_{H_2}H_2 + \dot{n}_{H_2O}H_2O + \dot{n}_{CH_4}CH_4 + \dot{n}_{C}C(\text{char}) + \dot{n}_{N_2} \quad \text{----4.6}$$

$C_6H_{HB}O_{OB}$ is the chemical formula of dry biomass in which HB and OB is obtained from proximate analysis. Char yield is obtained from ultimate analysis (non-equilibrium product). $\dot{w}$, $\dot{y}$ and $\dot{n}_i$ denote the molar flow rates of - moisture in feedstock, oxygen in the atmospheric air and products. Now, for given values of air–fuel ratio or equivalence ratio, biomass composition and moisture content, the quantity of product gases viz. CO, CO_2, H_2, H_2O, N_2 and char can be estimated based on the water–gas shift reaction and the atomic balances of Eq. 4.6. This estimation yields char as a non-equilibrium product. The quantity of the product gases estimated along with reaction temperature serves as initial condition of the reactants in the char reduction zone.

4.2.2 Reduction reactions

Four chemical reactions (CR1–CR4) are used to describe the reduction reaction zone. Prediction of the compositions of species viz., CO, CO_2, H_2, H_2O, CH_4, N_2 and charcoal or char is required. It is assumed that the char is consumed gradually in complete absence of oxygen due to char–gas reactions and gas–gas reactions as described by following chemical reactions.

CR1: Boudouard reaction: $C + CO_2 \leftrightarrow 2CO$ ----4.7

CR2: Water–gas (primary) reaction: $C + H_2O \leftrightarrow CO + H_2$ ----4.8

CR3: Methanation reaction: $C + 2H_2 \leftrightarrow CH_4$ ----4.9

CR4: Steam reforming reaction: $CH_4 + H_2O \leftrightarrow CO + 3H_2$ ----4.10

Ideal behaviour of all gaseous products are assumed. However, N_2 which although considered to be inert, dilutes the final energy density of gas. As the reactions (CR1–CR4) proceed, the temperature of char bed drops. This is due to nature of the reduction reaction of the char bed with the products of combustion. These reactions are generally heterogeneous endothermic. This causes a decrease in the char bed temperature. The reduction reactions (CR1–CR4) are considered for the modeling. The formulation of the Kinetic model for char reduction zone is described below.

4.2.3 Kinetic rate model of char reduction zone

The kinetic rate model is based on modeling approaches suggested by Sharma [32], Wang and Kinoshita [33]and Giltrap et al [34]. The reactions (CR1–CR4) are considered to describe the kinetic model of char reduction reactions. The apparent rate constants for each reaction are adopted from Giltrap et al [34]. The reactions are allowed to proceed up to the point where concentration of the reactants approach their equilibrium values. The reaction rates are then determined based on the deviation of the concentration of the reactant from the equilibrium values [33]. The reaction rates of each of the reactions is given by Eq. 4.11 – 4.14 respectively.

$$r_1 = C_{RF} k_1 \left(\chi_{CO_2} - \frac{\chi_{CO}^2}{K_{eq,1}} \right) \quad \text{----4.11}$$

$$r_2 = C_{RF} k_2 \left(\chi_{HO_2} - \frac{\chi_{CO}\chi_{H_2}}{K_{eq,2}} \right) \quad \text{----4.12}$$

$$r_3 = C_{RF} k_3 \left(\chi_{H_2}^2 - \frac{\chi_{CH_4}}{K_{eq,3}} \right) \quad \text{----4.13}$$

$$r_4 = C_{RF} k_4 \left(\chi_{H_2}^3 \chi_{CO} - \frac{\chi_{H_2O} \chi_{CH_4}}{K_{eq,4}} \right) \quad \text{----4.14}$$

where k_j is the reaction rate of the jth reaction which can be expressed using a Arrhenius-type temperature dependence given by Eq. 4.15.

$$k_j = A_j exp\left(\frac{-E_j}{R_u T}\right) \quad \text{----4.15}$$

where A_j is a pre-exponential factor and E_j is the activation energy for reactions j = 1–4 . The values of A_j and E_j is adopted from Wang and Kinoshita [33] and presented in Table 4.5. C_{RF} is the char reactivity factor. In the present analysis, a linearly varying C_{RF} has been used to incorporate the active sites present on char surface given by Eq. 4.16.

$$C_{RF} = 4.0012(10z) - 3.0012 \quad \text{----4.16}$$

where z is the displacement in the downward direction by the particle.

Table 4.5 Rate constant parameters of char reduction reactions

Reaction no. (j)	**A_j** [33]	**E_j (kJ/mol)** [33]
1	3.616×10^{1}	77.39
2	1.517×10^{4}	121.62
3	4.189×10^{-3}	19.21
4	7.301×10^{-2}	36.15

The char reduction zone can be divided into a number of control volumes axially. For the analysis, it is assumed that the net mass flow rate at entrance and exit of each control volume does not vary with time i.e. the local mass balance is steady in each control volume. This allows for the balance between the production of gas or species and consumption of char even though the mass balance of each species in each control volume is of unsteady or transient nature. The net rate of production of the gas or species can now be estimated in terms of the above reaction rates. The net production rate of each species can be used to compute outflow species concentration for known inflow concentration of each species and volume of each control volume as given by Eq. 4.17.

$$\dot{n}_{i,out} = \dot{n}_{i,in} + V_{CV,k} Rt_i \quad \text{----4.17}$$

where $\dot{n}_i$ represents the molar flow rate of the species *i*, $V_{CV,k}$ is the volume of the k^{th} control volume and Rt_i is the net production rate of species *i* in the control volume. Subscripts *in* and *out* represent the inflow and outflow plane flow rates, respectively.

4.2.4 Temperature simulation through energy balance

The temperature of the char bed is predicted based on an energy balance equation. The energy balance is based on the work of Sharma [32]. The equation takes into account the inflows and outflows of heat in a control volume due to flow of gases and feedstock. It also accounts for the heat transfer between adjacent control volumes due to conduction and radiation and the rate of endothermic heat absorption. The control volume considered in the analysis is shown in Fig. 4.6. The energy balance equation is given by Eq. 4.18.

$$\sum_{\text{react}} \dot{m}_i h_i + (-k_{\text{eff}} A \nabla T)_{\text{in}} - \dot{Q}_{\text{loss},k} - \dot{Q}_{\text{reac},k} = \sum_{\text{prod}} \dot{m}_i h_i + (-k_{\text{eff}} A \nabla T)_{\text{out}} \quad \text{----4.18}$$

$$h_i = \int_{T_A}^{T} C_{p_i} \mathrm{d}T \quad \text{----4.19}$$

where h_i is the sensible enthalpy change, which is based on char and combustion products at various stages of combustion; and k_{eff} is effective thermal conductivity of the char bed filled with gas mixture (based on Sharma's model). The bed porosity in biomass gasifiers varies from 0.5 at the top to 0.3 at the bottom [35]. An implicit function defining the variation in the bed porosity could not be determined. Therefore, an average bed porosity of 0.4 is assumed for the analysis. Char emissivity of 0.75 is used as reported by Ragland et al. [36]. The thermal interaction in adjacent upper and lower control volume (Fig. 4.7) is then estimated. $\dot{Q}_{\text{loss},k}$ is the rate of heat loss from k^{th} control volume, which is estimated based on a resistance network [32].

$\dot{Q}_{\text{reac},k}$ represents the rate of endothermic heat absorption occurring in the k^{th} control volume. This absorption rate can be based on the enthalpy of formation of the reactants and products given by Eq. 4.20.

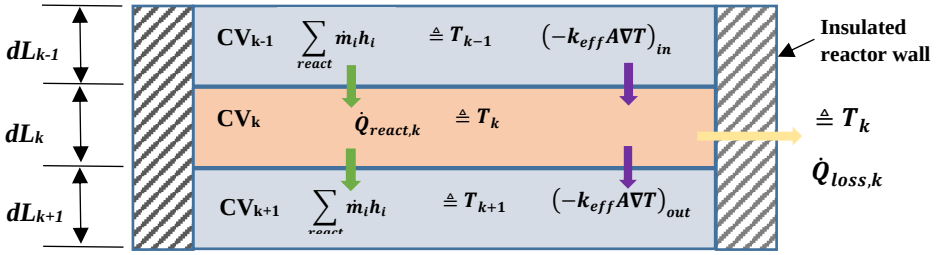

Fig. 4.7 Control volume used for heat transfer analysis
(Author's representation based on Sharma [32]**)**

$$\dot{Q}_{\text{reac},k} = \sum_{\text{react}} \dot{m}_i h^0_{f,i} - \sum_{\text{prod}} \dot{m}_i h^0_{f,i} \qquad \text{----4.20}$$

where, heat of formation of each constitute can be known from Turns [37].

The specific heat (kJ/kg K) and thermal conductivity (W/m K) of the char is based on the works of Ragland et al [36] and given by Eq. 4.21 and 4.22.

$$C_{p_{\text{char}}} = 1.39 + 0.00036T \qquad \text{----4.21}$$

$$k_{\text{char}} = 0.67S_{\text{char}} - 0.071 \qquad \text{----4.22}$$

where, S_{char} is the specific gravity of char.

The specific heats and thermal conductivity of gas mixture are then determined using Eq. 4.23 and 4.24 [38].

$$C_{p_{\text{gas-mixture}}} = \sum_{\text{gases}} Y_i C_{p_i} \qquad \text{----4.23}$$

$$k_{\text{mixture}} = \frac{\sum_{i=1}^{i} \chi_i k_i \,(\text{mw}_i)^{0.333}}{\sum_{i=1}^{i} \chi_i \,(\text{mw}_i)^{0.333}} \qquad \text{----4.24}$$

For determination of specific heat, the analysis adopts a polynomial equation fit given by Eq. 4.25 [39].

$$C_{p_i} = a_i + b_i T + c_i T^2 + d_i T^3 + e_i T^4 \qquad \text{----4.25}$$

Also, thermal conductivity is determined based on a polynomial curve fit given by Eq. 4.26 [40].

$$k_i = A_i + B_i T + C_i T^2 + D_i T^3 \qquad \text{----4.26}$$

4.2.5 Simulation and validation of the model

Simulations were performed to predict dry gas composition using the kinetic model for different feedstock. The information of inflow reactants to reduction model were obtained from upstream pyro-oxidation module based on the characteristics of the

feedstock. Values of air–fuel ratio or equivalence ratio, gas flow rate and moisture content of feedstock are required as input to the model. These values are obtained based on the feedstock characteristics and gasifier operating conditions. The simulation predicted the values of gas composition.

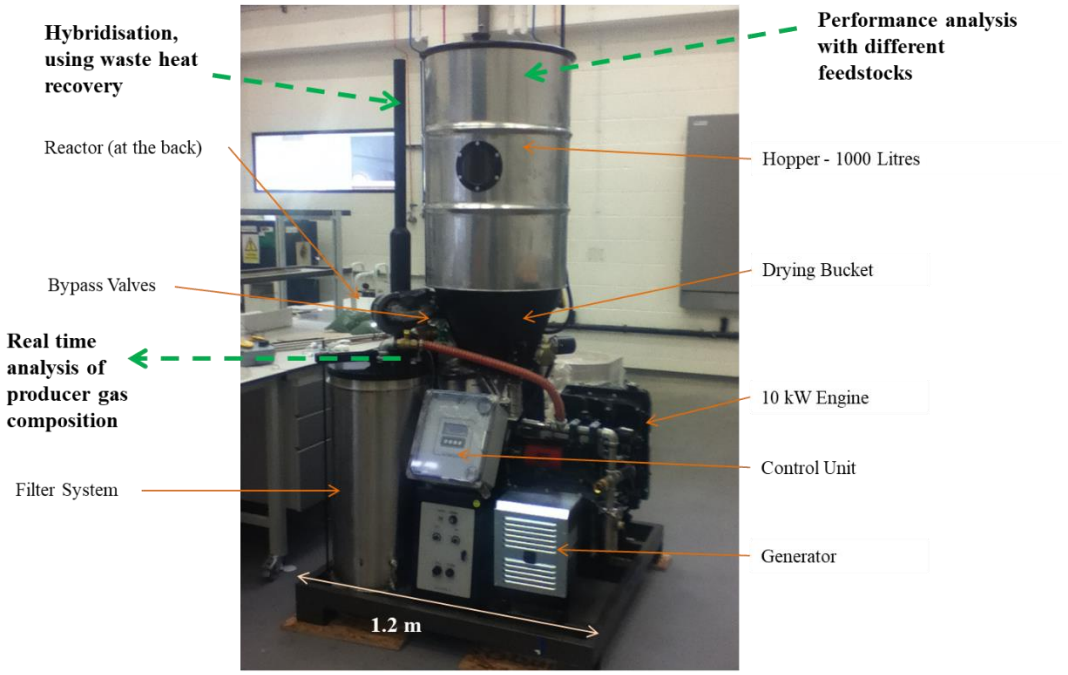

Fig. 4.8 Setup 1: 10 kW downdraft gasifier at University of Nottingham, UK

Fig. 4.9 Setup 2: 4 kW downdraft gasifier at Tezpur University, India

The theoretical predictions for gas composition were compared with the experimental data for validation. Two experimental setups were utilized for experimentation purpose. The first setup is of a 10 kW (Electrical) downdraft gasifier available at the Sutton Bonington campus of the University of Nottingham, UK as shown in Fig. 4.8. The second setup is that of a 4 kW (Thermal) downdraft gasifier available at the Department of Energy, Tezpur University, shown in Fig. 4.9. Locally available biomass were used as feedstock in the experimental facilities. Willow, Cedar and Eucalyptus were used as feedstock in the first setup whereas Gul Mohar and Dhaincha were used in the second setup. The characteristics of the biomass feedstock used for experimentation are summarized in Table 4.6.

Table 4.6 Characteristics of feedstock used for experimentation

Fuel	Moisture content (%)	Volatile matter (%)	Fixed carbon (%)	Ash (%)	Carbon (%)	Hydrogen (%)	Nitrogen (%)	Oxygen (%)
Willow*	10.95	64.38	19.03	5.64	50.36	6.74	1.12	41.64
Cedar*	9.92	67.79	17.57	4.73	53.30	6.20	0.10	40.40
Eucalyptus*	9.96	67.61	16.00	6.43	49.78	5.78	0.14	44.21
Gul Mohar**	13.33	61.01	13.08	10.93	43.08	5.63	1.18	50.11
Dhaincha**	13.58	85.63	12.53	1.84	45.240	6.060	0.560	46.300

* Experimentation in Setup 1
** Experimentation in Setup 2

The modelled values were compared with the experimental results. The comparison of the modelled values and the experimental values for different feedstock are shown in Fig. 4.10 – 4.14.

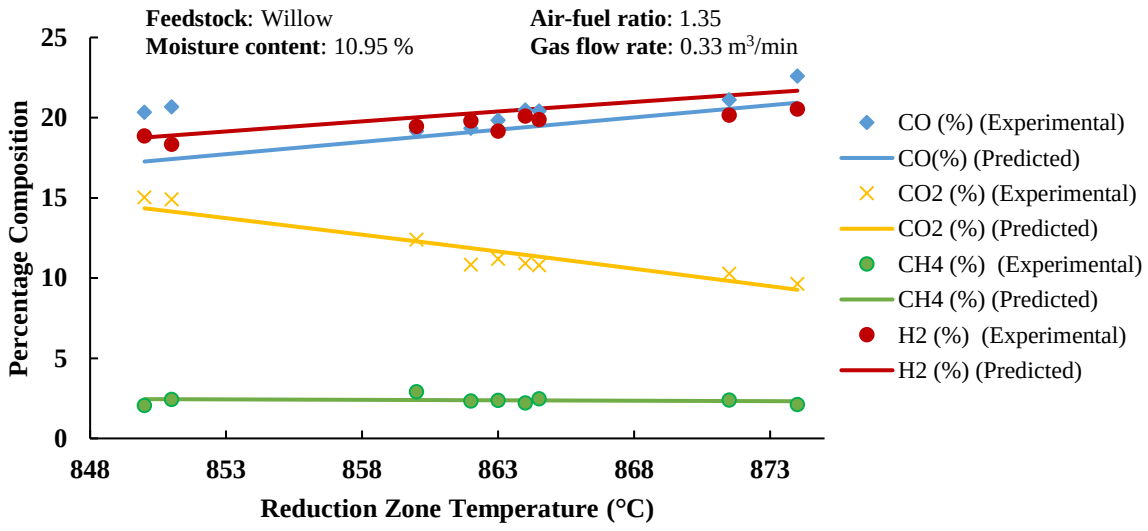

Fig. 4.10 Comparison of modelled and experimental gas composition using Willow

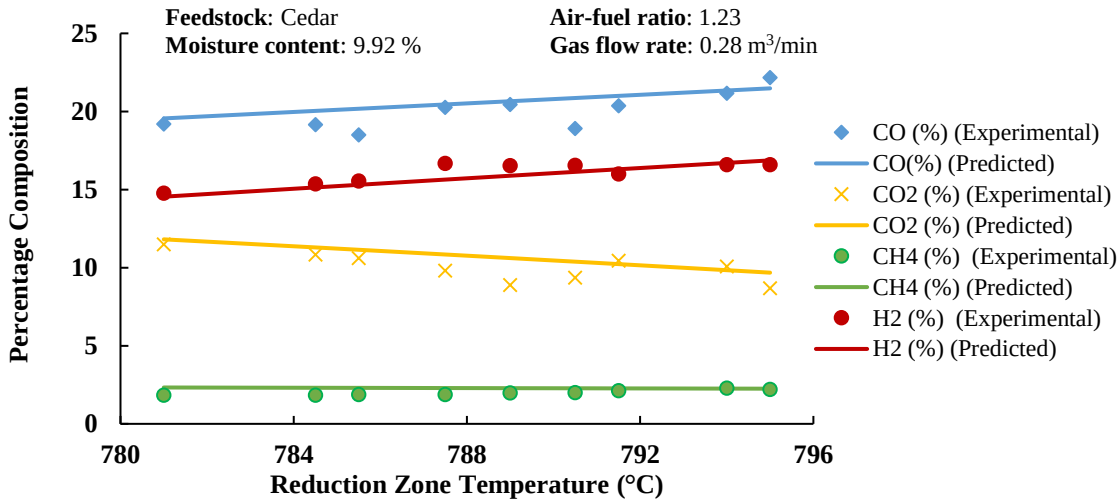

Fig. 4.11 Comparison of modelled and experimental gas composition using Cedar

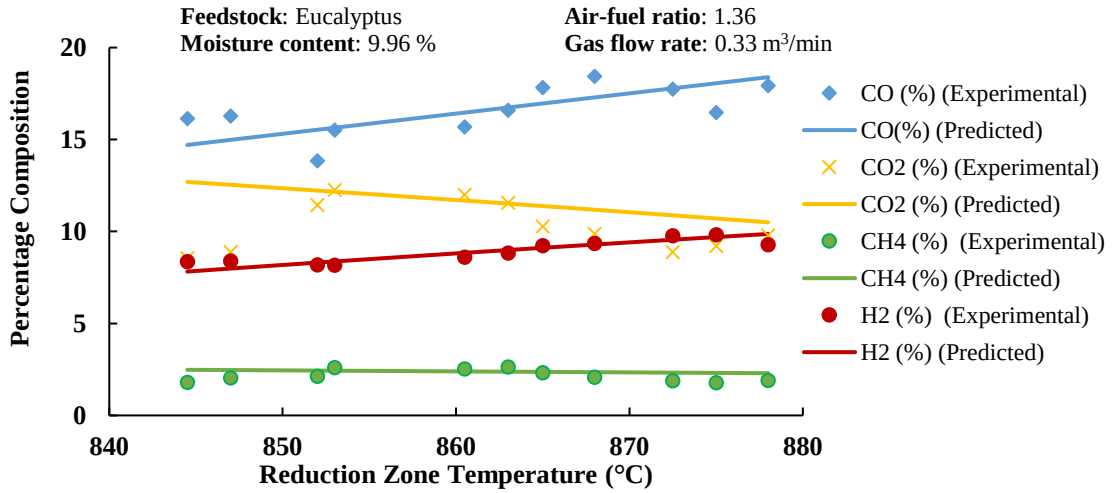

Fig. 4.12 Comparison of modelled and experimental gas composition using Eucalyptus

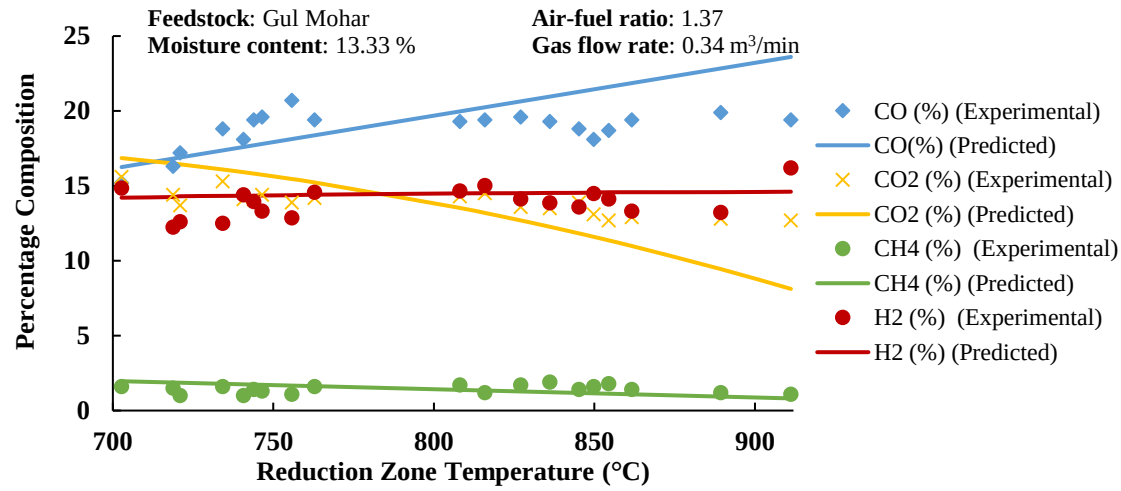

Fig. 4.13 Comparison of modelled and experimental gas composition using Gul Mohar

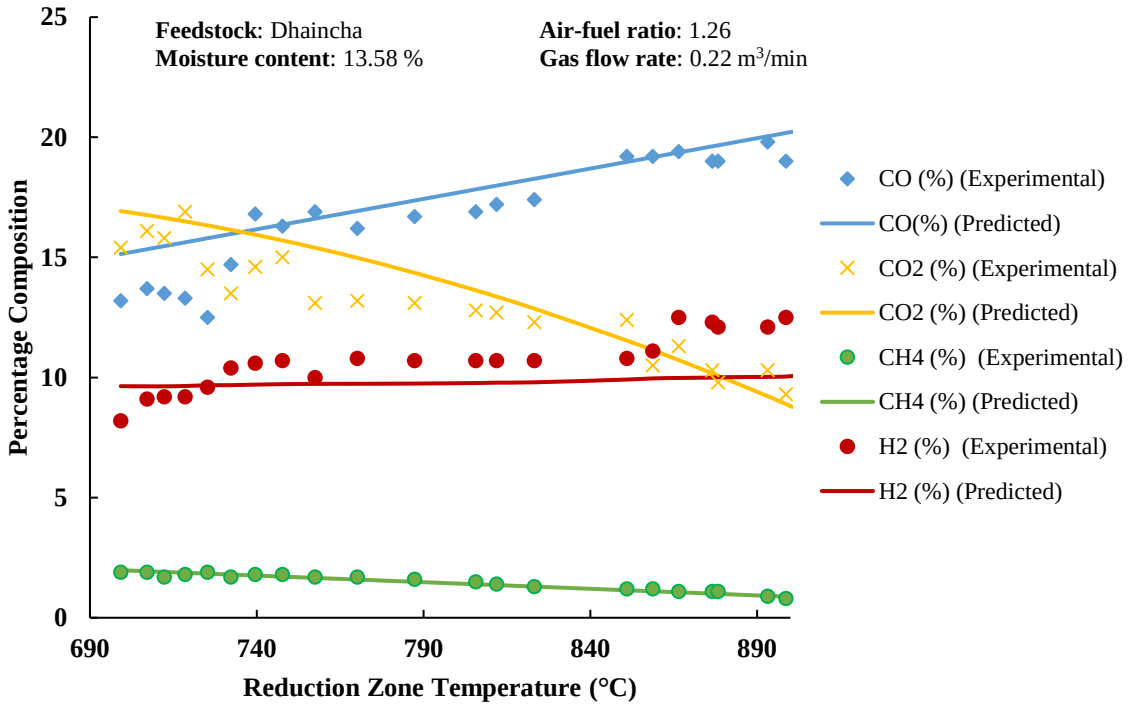

Fig. 4.14 Comparison of modelled and experimental gas composition using Dhaincha

The average relative error in the model prediction was considered as the validation criteria. The estimated average relative error in the model predictions are presented in Table 4.7.

Table 4.7 Average relative error in Kinetic model prediction (%)

Feedstock	CO	CO_2	CH_4	H_2
Willow	6.33	-0.47	-1.58	-3.44
Cedar	-5.17	-6.71	-1.45	4.45
Eucalyptus	-0.44	-6.85	-2.94	0.11
Gul Mohar	-4.23	2.29	-5.72	-4.43
Dhaincha	-5.97	-4.38	-0.57	7.61

It is observed that the model under-predicts the CO, CO_2 and CH_4 composition in almost every case with a maximum error of nearly 6%, 7% and 3% respectively. In the case of H_2 prediction there is mixed variation with a maximum error of 7.6% in the case of Dhaincha. The range of variations are however within acceptable limits establishing the validity of the model. The model is expected to exhibit good prediction ability.

4.2.6 Prediction of critical char bed length

The degree of char conversion has a strong influence on the energy balance [41]. Hence, for a given feedstock and operating conditions, there exists an optimal degree of char conversion which results in the maximum process efficiency. The length of the char bed at which all the char gets consumed is known as the critical char bed length (CCBL). CCBL is an important parameter, the knowledge of which is expected to be helpful in determining the size of a gasifier. An additional benefit of the model is its ability to predict the CCBL. The CCBL for varying ratings of the gasifier using different feedstock (Willow, Cedar and Eucalyptus) was predicted using the model. For the simulation, equivalence ratio, gas flow rate, moisture content and biomass composition were fixed for different ratings of the gasifier. An equivalence ratio of 1.3 was considered for each case. The gas flow rate was fixed at 0.25 m^3/min at 10 kW and increased in the ratio of corresponding increase in the gasifier rating. Moisture content and biomass composition were based on the characterisation of the feedstock. The results of the simulation are shown in Table 4.8. It may be observed that there is no significant variation in the predicted critical char bed length for a given rating of the gasifier using different feedstock. The results are expected to be useful helpful in determining the size of the reactor of a gasifier for a given rating. However, physical validation is required before generalising the results. Further research in this aspect is required to augment the prediction ability of the model.

Table 4.8 Prediction of critical char bed length

Power rating (kW)	Modelled critical char bed length (m)		
	Willow	Cedar	Eucalyptus
10	0.15	0.15	0.15
20	0.18	0.18	0.19
30	0.21	0.20	0.22
40	0.24	0.23	0.25

4.3 Summary

The necessity of modeling techniques for biomass gasification is augmented by the unavailability of experimental data based on different biomass feedstock for different ratings of the gasifier. The development of ANN and Kinetic model of fixed bed downdraft gasifier has been discussed. The developed models are expected to act as a generalised platform to predict gasification performance for a range of feedstock. The models are also expected to support the framework of a decision support system (DSS) for biomass gasification based energy generation. The development and utilization of a DSS for gasification based decentralised electricity generation is presented in the next Chapter.

REFERENCES

[1] Baruah, D., Baruah, D. C. Baruah, Hazarika, M. K. Artificial neural network based modeling of biomass gasification in fixed bed downdraft gasifiers. *Biomass and Bioenergy*, 98:264-271, 2017.

[2] Garson, G. D. Interpreting neural-network connection weights. *AI Expert*, 6(4):46-51, 1991.

[3] Antonopoulos, I.-S., Karagiannidis, A., Gkouletsos, A., Perkoulidis, G. Modelling of a downdraft gasifier fed by agricultural residues. *Waste Management*, 32:710–718, 2012

[4] Dogru, M., Howarth, C. R., Akay, G., Keskinler, B., Malik, A. A. Gasification of hazelnut shells in a downdraft gasifier. *Energy*, 27:415–427, 2002.

[5] Erlich, C., Fransson, T. H. Downdraft gasification of pellets made of wood, palm-oil residues respective bagasse: Experimental study. *Applied Energy*, 88:899–908, 2011.

[6] Gai, C., Dong, Y. Experimental study on non-woody biomass gasification in a downdraft gasifier. *International Journal of Hydrogen Energy*, 37:4935–4944, 2012.

[7] Janajreh, I., Shrah, M. Al. Numerical and experimental investigation of downdraft gasification of wood chips. *Energy Conversion and Management*, 65:783–792, 2013.

[8] Jaojaruek, K., Jarungthammachote, S., Gratuito, M. K. B., Wongsuwan, H., Homhual, S. Experimental study of wood downdraft gasification for an improved producer gas quality through an innovative two-stage air and premixed air/gas supply approach. *Bioresource Technology*, 102(7):4834-4840, 2011.

[9] Jordan, C. A., Akay, G. Effect of CaO on tar production and dew point depression during gasification of fuel cane bagasse in a novel downdraft gasifier. *Fuel Processing Technology*, 106:654–660, 2013.

[10] Kallis, K. X., Pellegrini Susini, G. A., Oakey, J. E. A comparison between Miscanthus and bioethanol waste pellets and their performance in a downdraft gasifier. *Applied Energy*, 101:333–340, 2013.

[11] Lapuerta, M., Hernández, J. J., Pazo, A., López, J. Gasification and co-gasification of biomass wastes: Effect of the biomass origin and the gasifier operating conditions. *Fuel Processing Technology*, 89:828–837, 2008.

[12] Lv, P., Yuan, Z., Ma, L., Wu, C., Chen, Y., Zhu, J. Hydrogen-rich gas production from biomass air and oxygen/steam gasification in a downdraft gasifier. *Renewable Energy*, 32(13):2173-2185, 2007.

[13] Tinaut, F. V., Melgar, A., Pérez, J. F., Horrillo, A. Effect of biomass particle size and air superficial velocity on the gasification process in a downdraft fixed bed gasifier. An experimental and modelling study. *Fuel Processing Technology*, 89(11):1076-1089, 2008.

[14] Sharma, A. K. Modeling and simulation of a downdraft biomass gasifier 1. Model development and validation. *Energy Conversion and Management*, 52:1386–1396, 2011.

[15] Sharma, A. K. Experimental investigations on a 20 kWe, solid biomass gasification system. *Biomass and Bioenergy*, 35:421–428, 2011.

[16] Sheth, P. N., Babu, B. V. Experimental studies on producer gas generation from wood waste in a downdraft biomass gasifier. *Bioresource Technology*, 100:3127–3133, 2009.

[17] Tinaut, F. V., Melgar, A., Pérez, J. F., Horrillo, A. Effect of biomass particle size and air superficial velocity on the gasification process in a downdraft fixed bed gasifier. An experimental and modelling study. *Fuel Processing Technology*, 89:1076–1089, 2008.

[18] steene, L. Van de., Tagutchou, J. P., Escudero Sanz, F. J., Salvador, S. Gasification of woodchip particles: Experimental and numerical study of char-H_2O, char-CO_2, and char-O_2 reactions. *Chemical Engineering Science*, 66:4499–4509, 2011.

[19] Varunkumar, S., Rajan, N. K. S., Mukunda, H. S. Experimental and computational studies on a gasifier based stove. *Energy Conversion and Management*, 53:135–141, 2012.

[20] Warnecke, R. Gasification of biomass: Comparison of fixed bed and fluidized bed gasifier. *Biomass and Bioenergy*, 18:489–497, 2000.

[21] Wei, L., Xu, S., Liu, J., Lu, C., Liu, S., Liu, C. A novel process of biomass gasification for hydrogen-rich gas with solid heat carrier: Preliminary experimental results. *Energy and Fuels*, 20(5):2266-2273, 2006.

[22] Brown, D., Fuchino, T., Maréchal, F. Solid fuel decomposition modelling for the design of biomass gasification systems. In *Computer Aided Chemical Engineering*, pages 1661-1666, Elsevier, UK, 2006.

[23] Krevelen, D. Van. Graphical statistical method for the study of structure and reaction processes of coal. *Fuel*, 29:269-284, 1950.

[24] Jenkins, B. M., Baxter, L. L., Miles, T. R., Miles, T. R. Combustion properties of biomass. *Fuel Processing Technology*, 54(1-3):17-46, 1998.

[25] Tabachnick, B. G., Fidell, L. S. *Using multivariate statistics*. Pearson, 5th Edition, 2012.

[26] Puig-Arnavat, M., Hernández, J. A., Bruno, J. C., Coronas, A. Artificial neural network models for biomass gasification in fluidized bed gasifiers. *Biomass and Bioenergy*, 49:279–289, 2013.

[27] Gai, C., Dong, Y. Experimental study on non-woody biomass gasification in a downdraft gasifier. *International Journal of Hydrogen Energy*, 37(6), 4935-4944, 2012.

[28] Chen, G., Andries, J., Luo, Z., Spliethoff, H. Biomass pyrolysis/gasification for product gas production: The overall investigation of parametric effects. *Energy Conversion and Management*, 44:1875–1884, 2003.

[29] Ghassemi, H., Shahsavan-Markadeh, R. Effects of various operational parameters on biomass gasification process: A modified equilibrium model. *Energy Conversion and Management*, 79:18–24, 2014.

[30] Reed, T. B., Markson, M. A Predictive Model for Stratified Downdraft Gasification of Biomass. In *Progress in biomass conversion*, 4: 217-254, Elsevier, UK, 2013.

[31] Shafizadeh, F. Pyrolytic Reactions and Products of Biomass. *In Fundamentals of Thermochemical Biomass Conversion*, pages 183-217, Springer, Dordrecht, 2011.

[32] Sharma, A. K. Equilibrium and kinetic modeling of char reduction reactions in a downdraft biomass gasifier: A comparison. *Solar Energy*, 82:918–928, 2008.

[33] Wang, Y., Kinoshita, C. M. Kinetic model of biomass gasification. *Solar Energy*, 51(1):19-25, 1993.

[34] Giltrap, D. L., McKibbin, R., Barnes, G. R. G. A steady state model of gas-char reactions in a downdraft biomass gasifier. *Solar Energy*, 74(1):85-91, 2003.

[35] Chen, J. S., Gunkel, W. W. Modeling and simulation of co-current moving bed gasification reactors - Part II. A detailed gasifier model. *Biomass*, 14(2):75-98, 1987.

[36] Ragland, K. W., Aerts, D. J., Baker, A. J. Properties of wood for combustion analysis. *Bioresource Technology*, 37(2):161-168, 1991.

[37] Turns, S. R. *An introduction to combustion : concepts and applications*. McGraw-Hill Education, 3rd Edition, 2011.

[38] Perry, R. H., Green, D. W. *Perry's Chemical Engineers' Handbook*. McGraw-Hill Education, 8th Edition, 2007.

[39] Thunman, H., Niklasson, F., Johnsson, F., Leckner, B. Composition of volatile gases and thermochemical properties of wood for modeling of fixed or fluidized beds. *Energy and Fuels*, 15(6):1488-1497, 2001.

[40] Reid, R. C., Sherwood, T. K., Street, R. E. *The Properties of Gases and Liquids*. McGraw-Hill Education, 5th Edition, 2009.

[41] Susastriawan, A. A. P., Saptoadi, H. Small-scale downdraft gasifiers for biomass gasification: A review. *Renewable and Sustainable Energy Reviews*, 76:989-1003, 2017.